Published in final edited form as:
J Nucl Med. 2012 April ; 53(4): 538–545. doi:10.2967/jnumed.111.096032.

^{11}C-Acetate PET/CT Imaging in Localized Prostate Cancer: A study with MRI and Histopathologic Correlation

Esther Mena[1], **Baris Turkbey**[1], **Haresh Mani**[2], **Stephen Adler**[1], **Vladimir A. Valera**[2], **Marcelino Bernardo**[1,3], **Vijay Shah**[1,3], **Thomas Pohida**[4], **Yolanda McKinney**[1], **Gideon Kwarteng**[1], **Dagane Daar**[1], **Maria L. Lindenberg**[1], **Philip Eclarinal**[1], **Revia Wade**[1], **W. Marston Linehan**[5], **Maria J. Merino**[2], **Peter A. Pinto**[5], **Peter L. Choyke**[1], and **Karen A. Kurdziel**[1]

[1]Molecular Imaging Program, NCI, NIH, Bethesda, MD, USA

[2]Laboratory of Pathology, NCI, NIH, Bethesda, MD, USA

[3]Imaging Physics, SAIC Frederick, Inc., NCI-Frederick, Frederick, MD, USA

[4]Division of Computational Bioscience, Center for Information Technology, NIH, Bethesda, MD, USA

[5]Urologic Oncology Branch, NCI, NIH, Bethesda, MD, USA

Abstract

This work characterizes the uptake of ^{11}C-Acetate in prostate cancer (PCa), benign prostate hyperplasia (BPH) and normal prostate tissue in comparison with multi-parametric MRI, whole mount histopathology and clinical markers, to evaluate its potential utility for delineating intra-prostatic tumors in a population of patients with localized PCa.

METHODS—39 men with presumed localized PCa underwent dynamic/static abdomen-pelvic ^{11}C-Acetate PET/CT for 30-minutes and 3T multi-parametric (MP) MRI prior to prostatectomy. PET/CT images were registered to MRI using pelvic bones for initial rotation-translation, followed by manual adjustments to account for prostate motion and deformation from the MRI endorectal coil. Whole-mount pathology specimens were sectioned using an MRI-based patient specific mold resulting in improved registration between the MRI, PET and pathology. ^{11}C-Acetate PET standardized uptake values were compared with MP-MRI and pathology.

RESULTS—^{11}C-Acetate uptake was rapid but reversible, peaking at 3–5 minutes post-injection and reaching a relative plateau at ~10 minutes. The average $SUV_{max(10–12min)}$ of tumors was significantly higher than that of normal prostate tissue (4.4±2.05, range 1.8–9.2 vs. 2.1±0.94, range 0.7–3.4; $p<0.001$); however it was not significantly different from benign prostatic hyperplasia (4.8±2.01; range 1.8–8.8). A sector-based comparison with histopathology, including all tumors > 0.5 cm, revealed a sensitivity and specificity of 61.6 % and 80.0 % for ^{11}C-Acetate PET/CT, and 82.3% and 95.1% for MRI, respectively. Considering only tumors >0.9 cm the ^{11}C-Acetate accuracy was comparable to that of MRI. In a small cohort (n=9), ^{11}C-Acetate uptake was independent of fatty acid synthase expression based on immunohistochemistry.

CONCLUSION—^{11}C-Acetate PET/CT demonstrates higher uptake in tumor foci than normal prostate tissue; however ^{11}C-Acetate uptake in tumors is similar to BPH nodules. While ^{11}C-Acetate PET/CT is not likely to have utility as an independent modality for evaluation of localized

Address correspondence to: Karen Kurdziel M.D. Molecular Imaging Program, National Cancer Institute, 10 Center Dr, MSC 1182, Bldg 10, Room B3B69, Bethesda, MD 20892-1088, karen.kurdziel@.nih.gov.

PCa, the high uptake in tumors may make it useful for monitoring focal therapy, where tissue damage after therapy may limit anatomic imaging methods.

Keywords

Prostate cancer; ^{11}C-Acetate PET; Multi-parametric prostate MRI

Prostate cancer (PCa) is the most frequently diagnosed cancer in men, and is the second most common cause of cancer death in men in developed countries (1). Early detection of PCa is important since cancer confined to the prostate gland is often curable. However, over-treatment is a concern since many of these cancers are not life threatening. Prostate-sparing, image guided therapies for localized PCa are under development in the hopes of reducing the morbidities associated with whole gland radiotherapy or radical prostatectomy. For such focal therapies to become accepted, accurate imaging methods of delineating PCa must be developed.

The ability to image localized PCa remains limited. When PCa is suspected based on high PSA or abnormal digital rectal examination, the diagnosis of PCa typically relies on blind, systemic biopsies obtained under ultrasound guidance. Ultrasound has limited sensitivity for PCa and is used primarily to guide the needle to pre-defined regions of the prostate gland (left and right, apex, mid, base) without knowledge of the actual location of the cancer.

MRI is the best available imaging technique for identifying PCa. Although T2 weighted (T2W) imaging has been the mainstay of prostate MRI, it is generally nonspecific for cancer, with low signal intensity being associated with prostatitis, scarring, or hyperplasia. Multi-parametric (MP) MRI has become popular, complementing T2Wimages with diffusion weighted (DWI), dynamic contrast enhanced (DCE), and MR spectroscopy imaging (MRSI) to improve diagnostic accuracy. MP-MRI remains imperfect with sensitivities/specificities ranging from 22–85% to 50–99% depending on technical factors and the composition of the study population (2).

Therefore, there is still a compelling need to more accurately identify PCa. Positron Emission Tomography (PET) has emerged as a promising imaging tool for cancer, however, the most commonly used PET radiotracer, ^{18}F-Fluoro-deoxy-glucose (FDG), has limited sensitivity for prostate cancer (3–4) due to low glucose consumption in early PCa, compounded by artifacts created from high bladder activity (5–6). Preliminary studies have demonstrated promising results with the PET agent, ^{11}C-Acetate, for the diagnosis of recurrent (7–8) or metastatic PCa (9), but its role in primary PCa detection and staging is less well established (10). Acetate is a naturally occurring fatty acid precursor that is converted to acetyl-CoA, a substrate for the tricarboxylic acid (TCA) cycle. Acetyl-CoA is incorporated into cholesterol and fatty acids and therefore ^{11}C-Acetate uptake is an indirect biomarker of fatty acid synthesis. Data suggests that ^{11}C-Acetate PET/CT imaging is useful in malignancies(11) including PCa (12–13). It has been suggested that since PCa relies more on fatty acid metabolism than on glycolysis (14), ^{11}C-Acetate may be a more appropriate imaging agent than FDG (15). Additionally, ^{11}C-Acetate shows minimal bladder activity.

We compared ^{11}C-Acetate PET/CT with 3T MP-MRI and whole-mount pathology in order to characterize ^{11}C-Acetate uptake in prostate tumors, relative to normal tissue and benign lesions in patients with localized PCa.

METHODS

Study Design and Patient Population

This is a HIPAA compliant, prospective, single institution study, approved by the local institutional review board (IRB). Inclusion criteria included: histologically proven adenocarcinoma of the prostate in patients who were eligible for prostatectomy. Exclusion criteria included contraindications to PET/CT or to MRI, contraindication to endorectal coil placement, prior radiation to the pelvis, and androgen deprivation therapy.

Between 2008 and 2010, forty patients signed consent, but only thirty-nine (mean age 58 years, range: 44–68) underwent ^{11}C-Acetate imaging. One was not imaged due to failed tracer synthesis. Data from the first patient, performed on a GE Advance camera using a ^{68}Ge source transmission scan for attenuation correction, was not evaluable due to inadequate registration between the transmission scan and MRI. All patients had MP-MRI, within 6-months of the ^{11}C-Acetate PET/CT. Following imaging, all patients underwent standard-of-care robotic assisted prostatectomy and lymph node dissection. There were 38 evaluable data sets; however the initial dynamic scans (0–6 minutes) were not available in 5 patients due to technical difficulties.

^{11}C-Acetate PET/CT Imaging Protocol

One patient was imaged on a GE LS Discovery in 2D acquisition mode, while the remaining 37 patients were imaged in 3D time of flight mode on a Philips Gemini TF camera, spatial resolution of 4.8mm at the center of the FOV. (16) The images were reconstructed using the default RAMLA iterative reconstruction (OSEM for the GE LS Discovery) (18), with standard corrections for randoms, scatter, attenuation, and normalization.

No specific patient preparation was required. ^{11}C-Acetate synthesis was conducted under IND #102705, using sterile conditions and an automated synthesis apparatus that utilized ^{11}C-carbon dioxide as a substrate. ^{11}C-Acetate was synthesized by reaction of methylmagnesium bromide with ^{11}C-Carbondioxide in tetrahydrofuran followed by hydrolysis and purification on small ion-exchange columns (17).

Following a low dose transmission CT scan of the abdomen and pelvis, each patient received an IV bolus injection of ^{11}C-Acetate, mean dose 39.8mCi (range 31.8–68.8), immediately followed by dynamic PET imaging of the lower pelvis (single bed position) for 6-minutes. Following this, alternating 2-minute static images were acquired at the initial bed position and at the contiguously superior bed position (lower abdomen) for the remaining 24-minutes of the study. Thus, static pelvic images were acquired at ~10, 16, 22 and 28-min post-injection while the static lower abdomen scans were performed at ~7, 13, 19 and 25-minutes post-injection. Vital signs were obtained prior to ^{11}C-Acetate injection and every 10 minutes during PET/CT imaging. The patients were queried regarding potential subjective adverse events during the scan and immediately thereafter.

MRI Protocol

MRI studies were performed using a combination of an endorectalcoil (*BPX-30, Medrad, Pittsburgh, PA*) and a 16-channel anterior cardiac coil (*SENSE, Philips Medical Systems, Best, Netherlands*) on a 3T magnet (*Achieva, Philips Medical Systems*) without prior bowel preparation. The endorectalcoil was inserted using a semi-anesthetic gel (*Lidocaine, AstraZeneca, US*) while the patient in the left lateraldecubitus position. The balloon surrounding the coil was distended with perfluorocarbon (*Fluorinert FC-770, 3M, St. Paul, MN*) to a volume of approximately 50mL to reduce susceptibility artifacts induced by air in the coil's balloon. The MRI protocol included tri-planar T2W turbo spin echo (TSE),

diffusion weighted (DW) MRI, 3D MR Spectroscopy Imaging (MRSI), axial pre-contrast T1W, axial 3D T1-weighted fast field echo dynamic contrast-enhanced (DCE) MRI sequences. Sequence parameters details were previously published (19).

Data Analysis

Histopathologic Analysis—After fixation the gland was sliced from the apex to base, at 6 mm intervals in the axial orientation of the MRI while supported inside a customized mold, which was designed for each patient prior to surgery, using *in-vivo* MRI, previously described (20). Further details regarding whole mount processing can be found in the Supplementary materials on-line.

Immunohistochemistry Analysis for Fatty Acid Synthase—Details are included in the Supplementary information available on-line.

Imaging Analysis

Visual Analysis: PET/CT scans were prospectively assessed by 2 experienced nuclear medicine physicians, and MRI scans were prospectively assessed by two experienced radiologists, blinded to the other modality and histopathology results.

Lesion-based Analysis: On the PET images, volumes of interest (VOIs) were created in visually identified abnormal foci of ^{11}C-Acetate uptake (greater than adjacent background). A small VOI within a homogeneous region of an iliac vessel was used as the vascular input function. VOIs within a homogeneous portion of muscle and normal prostate were used to create a reference tissue TACs. PET data were analyzed quantitatively by calculating SUV_{max}, for each lesion and SUV_{mean} for the input function and reference tissues, and by the Logan (21)and Patlak (22) reference-region-based graphical analyses (to assess reversible and irreversible tracer binding respectively).

On MRI, a “visible index lesion” was defined as a well circumscribed, round-ellipsoid, with low-signal-intensity on T2W-MRI and apparent diffusion coefficient (ADC) maps of DW-MRI (19). 3D-MRSI was analyzed by acquiring choline/citrate (Cho/Cit) ratios within index lesions. Voxels were considered abnormal when the (Cho/Cit) ratio was 3 or more standard deviations (SD=0.13+/−0.081) above the mean healthy Cho/Cit ratio value (≥0.373), based on a previous evaluation of 433 healthy, biopsy negative voxels from the peripheral zone and 44 additional voxels from biopsy positive cancers (19). DCE-MRI was evaluated subjectively for early and intense enhancement followed by rapid washout, characteristic of PCa (19). The overall sensitivities and specificities reported reflect the qualitative assessment of combined MP-MRI readout.

VOIs in tumor-containing and normal prostate tissue were defined using T2W-MRI. These MRI VOIs were also applied to the reoriented ^{11}C-Acetate PET/CT images, and SUV_{max} TACs for any lesions seen on MRI, but not on PET, were created.

Sector-based Analysis: Using the MRI as an anatomic map, sector-based analysis was also performed. The prostate was segmented into 5 levels in the superior-inferior axis, and 4 VOIs (left and right, anterior and posterior quadrants) were created in each axial plane level resulting in a total of twenty sectors for each patient.

The sector VOIs were applied to the images and the previously drawn lesion-based VOIs were overlaid on these 20 sectors using the co-registered MRI and PET. (MIM 4.2/5.1, MIM Software Inc. Cleveland, OH, USA)

Based on the mutual alignment of the histopathology, MRI and PET/CT VOIs, each sector was assigned as True Positive, True Negative, False Positive, and False Negative according to pathology results for both MRI and PET/CT interpretations. The tumor focus was considered correlated when it was located either in the same sector or an immediately adjacent sector ('neighboring' region) as the corresponding pathologic sector.

For the MRI analysis, a sector was considered tumor positive when the whole or any part of the lesion was within the sector. For PET analysis, a small region of interest composed of the "hottest" 20% of lesion-defined pixels (using an 80% maximum pixel threshold) spanned multiple sectors, all of the affected sectors were considered positive.

Sensitivity, specificity and accuracy of MRI and ^{11}C-Acetate PET/CT interpretations with respect to histopathology were calculated.

Imaging Data and Histopathology Correlation

There are inherent difficulties in correlating imaging findings with histopathology. Following prostatectomy, the prostate gland may deform, and after fixation, variable shrinkage may occur; therefore, sectioning of the fixed specimen does not necessary correlate exactly with images in terms of thickness or slicing plane, resulting in slight mismatches between pathology and imaging. We reduced this problem by using a customized mold for each patient, which were created using the MRI prior to surgery. The mold insured that the specimens were sectioned as close to the same plane as the imaging as possible. Thus, the PET and MRI scans were aligned with whole mounted prostate specimens with the highest possible accuracy. PET/CT images were registered and fused in the same plane as the MRI using MIM 4.2/5.1, the transmission CT was grossly registered to the MRI, using the pelvic bones for initial rotation-translation. The PET was then brought into the imaging space of the resultant CT/MRI fusion, yielding registration of the PET/CT and MR. Manual adjustments were made in the MRI/PET registration to account for prostate motion and deformation due to the MRI endorectal coil.

Only tumors >0.5 cm were analyzed, which included all dominant tumors. Patients were divided into prognostic groups: low risk, Gleason score equal to or less than 3+4; and high risk, Gleason score equal to or greater than 4+3. Patients Serum PSA based grouping were also made: less than 4ng/ml, between 4 and 10ng/ml, and higher than 10ng/ml.

Statistical Analysis

SUV_{max} measurements of ^{11}C-Acetate PET/CT imaging were obtained in tumor and non-tumor regions and compared using a paired two-sided t-test. Results were presented as mean ± 1SD (p values < 0.05 were considered to represent a significant difference).

The diagnostic accuracy of ^{11}C-Acetate PET/CT imaging in PCa was compared with MP-MRI using the sector-based analysis, generating receiver-operating-characteristic (ROC) curves (plots of 1-specificity versus sensitivity) for both modalities. In addition, the SUV of ^{11}C-Acetate uptake was correlated with histopathologic Gleason score and PSA values, using a Spearman rank correlation.

RESULTS

Clinical Findings

The final study population consisted of 38 PCa patients (mean age 58 years; range, 44 to 68) who underwent radical prostatectomy within a mean of 10.5 days (range, 1 to 34 days) of ^{11}C-Acetate PET/CT imaging. The mean interval between MRI and prostatectomy was

54 days (range, 2 to 155 days). ^{11}C-Acetate injections were well-tolerated by all patients with the only reported adverse event recorded being a grade 1 taste disturbance during the infusion in 10 patients, which resolved spontaneously. At the time of ^{11}C-Acetate PET scanning, the mean PSA level was 7.03 ± 8.88 ng/ml, ranging from 1.07 ng/mL to 53.5 ng/mL; fifteen patients with PSA< 4 ng/ml, nineteen with PSA between 4 and 10 ng/ml and five with PSA > 10 ng/ml. A total of 167 tumor foci were histopathologically identified in 38 patients, with 80 of these foci (48%) larger than 0.5 cm. While six patients demonstrated more than one smaller tumors foci (less than 0.5 cm) aggregated within the same sector area, such aggregates were not identified on imaging. Gleason scoring of the tumor lesion(s) varied between 3+3 and 4+5. Considering all tumors identified on pathology: thirteen tumors were scored as 3+3, forty-five as 3+4, four as 4+3, eleven as 4+4, and seven as 4+5. All pelvic lymph nodes were negative by clinical imaging criteria. Following prostatectomy, microscopic involvement of one lymph node was found in one patient.

Diagnostic Accuracy Of PET/CT and Multiparametric MRI

Visual Analysis—On a per patient basis, ^{11}C-Acetate PET/CT was positive in at least one lesion in 34 of the 38 patients (89%), whereas MP-MRI was positive in 37 of the 38 patients (97%).

Lesion Based Analysis—Lesion-based analysis, revealed 47 true positive tumor sites, 17 false negative sites and 37 false positive sites for ^{11}C-Acetate PET, resulting in a sensitivity of 73.4%. For MP-MRI, 54 sites were identified as true positive for tumor, 7 false negative and 3 false positive, with resultant sensitivity of 88.5%. Functional MP-MRI modalities; DW-MRI, DCE-MRI and MRSI, revealed sensitivities of 80%, 55%, and 27%, respectively. ^{11}C-Acetate PET/CT identified 5 tumor foci that were not seen with any of the MRI modalities, whereas MRI localized 15 tumor sites that were not identified on ^{11}C-Acetate PET/CT.

Sector Based Analysis—In 20 sectors, ^{11}C-Acetate PET/CT showed sensitivity, specificity, positive predictive value (PPV), and negative predictive values (NPV) of 61.6%, 80.0%, 56%, and 88% respectively. On MP-MRI, these values were 82.3%, 95.1%, 91% and 89%, respectively.

In pathologically confirmed tumors with visible ^{11}C-Acetate uptake, the mean tumor volume, measured using a volumetric region of interest on MRI, was larger than tumors without visible uptake: 3.1±4.4 ml vs. 0.6±0.7 ml. This difference was statistically significant (p=<0.001); although there was overlap between groups. Receiver operator curve (ROC) analysis showed the disparity between MRI and ^{11}C-Acetate PET/CT to be less, with improved discrimination for both modalities, for lesions >0.9 cm (Supplemental FigureS1).

Quantitative analysis—Representative TACs (Figure 1) showed rapid ^{11}C-Acetate uptake in the prostate, peaking ~ 3 to 5 minutes post injection, followed by a relative plateau approximately 10 minutes post injection. The average $SUV_{max(10–12min)}$ of the histopathologically confirmed tumors was significantly higher (4.4±2.05, range 1.8–9.2) than that of normal prostate tissue (2.1±0.943; range 0.7–3.4) (p<0.0001); however foci of benign prostatic hyperplasia (BPH) also showed high ^{11}C-Acetate uptake, (average SUV_{max} of 4.8±2.01; range 1.8–8.8), which was not significantly different from that of tumor (p=0.65) (Figure 4A). Additionally, ^{11}C-Acetate PET/CT identified two foci, SUV_{max} of 3.8 and 2.9, shown to be prostatitis on histopathology.

The TACs were evaluated using a graphical analysis for reversible tracers (Logan plot), with the slope estimating the distribution volume ratio (DVR) (21), a linear function of receptor

availability, and Patlak graphical analysis for irreversible tracers (22), with the y-intercept representing the tracer influx rate.

The Logan plots became linear at ~3 minutes post injection consistent with reversible binding (Table 1 and Supplemental Figure S2). The average volume of distribution (Vd), representing both specific and non-specific binding, estimated by the slope of the linear portion of the Logan plot, was 3.0, (r=0.999), for the dominant tumors (n=38), 3.4, (r=0.997) for BPH (n= 21) and 1.4, (r=.997) for normal prostate (n=38). Using normal prostate as a reference tissue for tissue specific binding, resulted in distribution volume ratios (DVR) of 2.0, (r=0.999), and 2.3, (r=0.999) for tumor and BPH respectively. The Patlak plots were not linear, suggesting minimal if any irreversible binding.

Comparison Between ^{11}C-Acetate Uptake And Clinical Markers

No significant correlation was observed between ^{11}C-Acetate SUV_{max} and serum PSA levels (r= −0.128) using Spearman correlation. SUV_{max} did not differ between patients with low or high PSA levels: average SUV_{max} of 3.7±2.0 for PSA level <4 ng/ml, 4.9±2.3 for PSA between 4 to 10 ng/ml, and 5.1±0.8 for PSA > 10 ng/ml (p=0.407) (Figure 4B). There was no significant correlation between SUV_{max} and tumor foci Gleason scores (r=0.187). Similarly no significance was found grouping the tumors based on Gleason scores 3+4 and below: average SUV_{max} 4.2±1.8; 4+3 and above: average SUV_{max} 4.9±3.1 (p=0.55) (Figure 4C). Immunohistochemistry (IHC) analysis for FAS revealed no visible difference in staining intensity between tumors with high (visible) and low ^{11}C-Acetate uptake (Figure 5).

DISCUSSION

While PCa is a multifocal disease, not all prostate tumors have a poor prognosis, and treatment is dictated by the dominant tumor with the highest clinical grade. If ^{11}C-Acetate PET/CT was able to delineate poorer prognostic lesions in the setting of localized PCa, perhaps, it could be used to perform targeted biopsies (rather than sextant standard-of-care biopsies performed currently) or to direct focal therapy. As organ sparing approaches are being explored, the challenge of monitoring such therapy following tissue ablation has become more apparent. Availability of a non-invasive specific marker not affected by anatomic distortions would be helpful.

In a study of in 22 patients with histologically confirmed PCa, Oyama et. al. demonstrated the feasibility of using ^{11}C-Acetate PET to visualize primary PCa (8), with positive accumulation occurring in all primary tumors, albeit with variable SUV values (3.3–10), on static images performed 10–20 minutes post-injection. As only the known tumors were evaluated, their study did not include data on ^{11}C-Acetate uptake in benign prostate conditions, and the PET region of interest was based on visual analysis. Similar results were published by Kato et al (23), who reported lower but overlapping SUVs for BPH (mean SUV of 2.1±0.6), and for prostate tumors (mean SUV of 1.9±0.6); however not all tumors, and none of the BPH foci had histological confirmation (23). Their SUVs (measured between 16 and 20 minutes post-injection) in tumor foci were lower than our study, which is likely due to the use of different region of interest and/or data analysis methods. Tumor sizes were not provided in either study.

For our primary analysis we only considered foci which were >0.5 cm (within the spatial resolution of all imaging systems utilized) on pathology (n=80), and report SUV_{max} values determined at the beginning of the uptake plateau: between 10 and 12-minutes post injection. Our results showed ^{11}C-Acetate uptake to be equal between benign and malignant processes. The $SUV_{max(10–12min)}$ of histopathologically defined tumors ranged from 1.8 to

9.2 with an average value of 4.4±2.0, overlapping that of BPH nodules, mean 4.8±2.0, range 1.8 to 8.8. The mean normal prostate tissue uptake was lower, at 2.1±0.9.

On a lesion-by-lesion visual analysis, ^{11}C-Acetate PET/CT showed a sensitivity of 73.4% while the sensitivity for MP-MRI was 88.5%, diffusion weighted imaging (DWI) was 80%, DCE-MRI was 55%, and MRSI was 27% placing ^{11}C-Acetate PET/CT between DWI and DCE-MRI in relative sensitivity. ^{11}C-Acetate PET/CT identified 5 tumors that MRI did not; however MRI identified 15 tumors not seen on PET. Using a sector-based analysis, where each lesion was assigned to one of 20 anatomically based sectors, resulted in sensitivity and specificity values for ^{11}C-Acetate PET/CT of 61.6% and 80% respectively while the same values for MP-MRI were 82.3% and 95.1%. ^{11}C-Acetate PET showed 124 false positive sectors due to its uptake in BPH and 62 false negative sectors; however, interpreting these foci in light of the MRI findings led to a reclassification of positive PET findings as non-malignant foci in 30 sites of BPH, which were all confirmed by histopathology.

Both of these analyses demonstrated ^{11}C-Acetate PET/CT to be inferior to MP-MRI for lesions >0.5 cm; however, this gap narrowed when considering only lesions >0.9 cm. The results of the ROC analysis showed that both modalities performed better on larger lesions, with sensitivities and specificities of 93.5% [204/218 positive sectors] and 84.9% [477/562 negative sectors] for MRI and 89.3% [195/218 positive sectors] and 89.9% [505/562 negative sectors] for PET in lesions greater than 0.9 cm.

As expected, tumors with visible uptake on ^{11}C-Acetate PET/CT were larger (3.1 ± 4.4 ml) than those without visible uptake (0.6 ± 0.07); $p<0.001$. However, it should be noted that the index tumor (largest tumor with the worst Gleason score) is the most significant with regard to progression of PCa and its response to treatment carries the most clinical importance(24). While partial volume correction may have increased the absolute tumor SUV values, it would not have increased their visibility.

While dynamic uptake of ^{11}C-Acetate in PCa was described by Schiepers et al(25) in ten patients and by Kato et. al (23) in six patients, neither group compared the results with spatially mapped histopathology. Kato et al used an early (6–10 minute) to late (16–20 minute) ^{11}C-Acetate uptake ratio, which was near unity for normal, BPH and tumor. Schiepers et. al. implemented a compartmental model with both bound and free compartments within the prostate, as well as Patlak graphical analysis (assuming irreversible kinetics). Their TACs demonstrated rapid clearance from the blood with peak uptake in the prostate tissue at around 5-minutes, followed by a plateau. This is comparable to our results, which show a peak uptake around 3–5 minutes; however in our data, this is immediately followed by a decrease in activity due to tracer washout just prior reaching a plateau. As the Logan plots became linear at ~3 minutes, indicating equilibrium with blood had been reached; this early peak was due to initial tumor perfusion. Following that peak, our TACs also demonstrate a slow washout of tracer, similar to that of blood clearance, beginning after 10 minutes. These discrepancies in the TACs, in comparison with previously publish results, can probably be explained by the differences in VOI definition; we used the absolute SUV_{max} of the VOI defined by the extent of involvement on whole mount histopathology. Use of the SUV_{mean} would likely have resulted in inclusion of non-tumorous tissue due inherent mis-registration. In contrast, without the advantage of PET/CT and registration capabilities, Schiepers et al (25) used a VOI based on a 50% maximum pixel threshold, which likely included normal prostate tissue, thereby diluting the value (normal prostate SUV and tumor SUV within the VOI). Additionally, they applied partial volume correction to the input function and not to the tumors. We chose not to apply a partial volume correction as the size of the lesions and iliac vessels were similar and the corrections would likely cancel each other out.

Interestingly, Schiepers et al (25) report Patlak graphical analysis parameters for the data between 7 and 20 minutes (assuming irreversible binding); however the Ki values (a measure of net tracer flux into the tumor) were quite low, correlation coefficients were not provided. In our data, while a relative plateau is reached after 10 minutes, this is followed by a slow decrease in activity, similar to the blood clearance, suggesting that transfer of tracer from the tumor back to the blood is not negligible and the binding is reversible. Patlak plots of our data were not linear or showed minimally negative slopes. The results of our Logan graphical analysis resulted in excellent linearity (r-values (correlation coefficients) =0.99). The slope of the Logan plot represents the volume of ^{11}C-Acetate distribution (Vd) with respect to blood and these values for tumor, BPH and normal prostate are listed in Table 1. We also performed a reference-tissue based Logan analysis using the normal prostate as the reference tissue to estimate the distribution volume ratio (DVR) between the target lesion and the reference tissue. This value is an indicator of lesion-specific binding (relative to the normal prostate), and eliminates the contribution of the differential organ perfusion and non-specific binding. The DVR values for tumor and BPH are similar. While the absolute values of our parameters do not match those of Schiepers et al, a similar uptake in BPH and tumors was found.

Regarding correlation between ^{11}C-Acetate PET and MRI, Jambor et al found that ^{11}C-Acetate PET/CT detected localized PCa with a sensitivity, specificity and accuracy of 80%, 29%, 71%, respectively, comparable to contrast-enhanced MRI. However, neither PET SUVs nor the MRSI (choline + creatine + polyamines) to citrate ratios were included. Oyama et al. (9), found no correlation between clinical parameters and ^{11}C-Acetate uptake.

^{11}C-Acetate tumor uptake is thought to be due, in part, to increase lipid synthesis. To explore this potential mechanism, we performed IHC staining for fatty acid synthase on biopsy samples in a subset of 9 subjects. Levels of staining were high in all tumors, regardless of SUV, indicating that fatty acid synthesis expression is not sufficient to explain the ^{11}C-Acetate mechanism of uptake in humans. This finding is not surprising as previous work from Liu et al. showed significant overlap of FAS expression in tumor, BPH, and normal prostate (14).

One source of error in our analysis involves our method of image registration. We fused PET, MRI and histopathology data using a semi-automated mutual information technique followed by minor manual adjustments. This introduced a subjective component in accounting for gland deformation. More robust CT to MRI deformable registration algorithms are needed to register PET/CT with MRI. Alternatively, the recent development of PET/MRI scanners may obviate the need for registration.

CONCLUSION

We have characterized the kinetic uptake of ^{11}C-Acetate uptake in tumor, BPH and normal prostate tissue in localized PCa, with correlation to multi-parametric MRI, whole mount histopathology, fatty acid synthase expression and clinical markers. ^{11}C-Acetate PET/CT demonstrates higher uptake in intra-prostatic tumor foci than normal prostate tissue; however uptake in tumors was similar to BPH nodules. While ^{11}C-Acetate PET/CT is not likely to have utility as an independent modality for evaluation of localized PCa, the high differential uptake in tumors, with respect to normal prostate, may make it useful for monitoring focal therapy, where post-treatment anatomical changes may limit MRI's utility.

Supplementary Material

Refer to Web version on PubMed Central for supplementary material.

Acknowledgments

This research was supported by the Intramural Research Program of the NIH, National Cancer Institute, Center for Cancer Research. We would like to thank Michael Channing PhD and the NIH Clinical Center PET Department for providing the C-11 Acetate.

References

1. Damber JE, Aus G. Prostate cancer. Lancet. 2008; 371(9625):1710–1721. [PubMed: 18486743]
2. Turkbey B, Albert PS, Kurdziel K, Choyke PL. Imaging localized prostate cancer: current approaches and new developments. AJR Am J Roentgenol. 2009; 192(6):1471–1480. [PubMed: 19457807]
3. Liu IJ, Zafar MB, Lai YH, Segall GM, Terris MK. Fluorodeoxyglucose positron emission tomography studies in diagnosis and staging of clinically organ-confined prostate cancer. Urology. 2001; 57(1):108–111. [PubMed: 11164153]
4. Hofer C, Laubenbacher C, Block T, Breul J, Hartung R, Schwaiger M. Fluorine-18-fluorodeoxyglucose positron emission tomography is useless for the detection of local recurrence after radical prostatectomy. Eur Urol. 1999; 36(1):31–35. [PubMed: 10364652]
5. Takahashi N, Inoue T, Lee J, Yamaguchi T, Shizukuishi K. The roles of PET and PET/CT in the diagnosis and management of prostate cancer. Oncology. 2007; 72(3–4):226–233. [PubMed: 18176088]
6. Schoder H, Larson SM. Positron emission tomography for prostate, bladder, and renal cancer. Semin Nucl Med. Oct; 2004 34(4):274–292. [PubMed: 15493005]
7. Sandblom G, Sorensen J, Lundin N, Haggman M, Malmstrom PU. Positron emission tomography with C11-acetate for tumor detection and localization in patients with prostate-specific antigen relapse after radical prostatectomy. Urology. 2006; 67(5):996–1000. [PubMed: 16698359]
8. Oyama N, Miller TR, Dehdashti F, et al. 11C-Acetate PET Imaging of Prostate Cancer: Detection of Recurrent Disease at PSA Relapse. J Nucl Med. 2003; 44(4):549–555. [PubMed: 12679398]
9. Oyama N, Akino H, Kanamaru H, et al. 11C-acetate PET imaging of prostate cancer. J Nucl Med. 2002; 43(2):181–186. [PubMed: 11850482]
10. Jambor I, Borra R, Kemppainen J, et al. Functional imaging of localized prostate cancer aggressiveness using 11C-acetate PET/CT and 1H-MR spectroscopy. J Nucl Med. 2010; 51(11): 1676–1683. [PubMed: 20956477]
11. Liu RS. Clinical Application of [C-11]acetate in Oncology. Clin Positron Imaging. 2000; 3(4):185. [PubMed: 11150788]
12. Vavere AL, Kridel SJ, Wheeler FB, Lewis JS. 1-11C-acetate as a PET radiopharmaceutical for imaging fatty acid synthase expression in prostate cancer. J Nucl Med. 2008; 49(2):327–334. [PubMed: 18199615]
13. Yoshimoto M, Waki A, Yonekura Y, et al. Characterization of acetate metabolism in tumor cells in relation to cell proliferation: Acetate metabolism in tumor cells. Nucl Med Biol. 2001; 28(2):117–122. [PubMed: 11295421]
14. Liu Y. Fatty acid oxidation is a dominant bioenergetic pathway in prostate cancer. Prostate Cancer Prostatic Dis. 2006; 9(3):230–234. [PubMed: 16683009]
15. Shreve P, Chiao PC, Humes HD, Schwaiger M, Gross MD. Carbon-11-Acetate PET Imaging in Renal-Disease. J Nucl Med. 1995; 36(9):1595–1601. [PubMed: 7658216]
16. Surti S, Kuhn A, Werner ME, Perkins AE, Kolthammer J, Karp JS. Performance of Philips Gemini TF PET/CT scanner with special consideration for its time-of-flight imaging capabilities. J Nucl Med Mar. 2007; 48(3):471–480.
17. Kruijer PS, Terlinden T, Mooij R, Visser FC, Herscheid JDM. A Practical Method for the Preparation of [C-11] Acetate. Appl Radiat Isot. 1995; 46(5):317–321.
18. Browne J, DePierro AR. A row-action alternative to the EM algorithm for maximizing likelihoods in emission tomography. IEEE T Med Imaging. 1996; 15(5):687–699.
19. Turkbey B, Pinto PA, Mani H, et al. Prostate cancer: value of multiparametric MR imaging at 3 T for detection--histopathologic correlation. Radiology. 2010; 255(1):89–99. [PubMed: 20308447]

20. Shah V, Pohida T, Turkbey B, et al. A method for correlating in vivo prostate magnetic resonance imaging and histopathology using individualized magnetic resonance-based molds. Rev Sci Instrum. 2009; 80(10):104301. [PubMed: 19895076]
21. Logan J, Fowler JS, Volkow ND, Wang GJ, Ding YS, Alexoff DL. Distribution volume ratios without blood sampling from graphical analysis of PET data. J Cereb Blood Flow Metab. 1996; 16(5):834–840. [PubMed: 8784228]
22. Patlak CS, Blasberg RG. Graphical evaluation of blood-to-brain transfer constants from multiple-time uptake data. Generalizations. J Cereb Blood Flow Metab. 1985; 5(4):584–590. [PubMed: 4055928]
23. Kato T, Tsukamoto E, Kuge Y, et al. Accumulation of [C-11]acetate in normal prostate and benign prostatic hyperplasia: comparison with prostate cancer. Eur J Nucl Med Mol Imaging. 2002; 29(11):1492–1495. [PubMed: 12397469]
24. Wise AM, Stamey TA, McNeal JE, Clayton JL. Morphologic and clinical significance of multifocal prostate cancers in radical prostatectomy specimens. Urology. 2002; 60(2):264–269. [PubMed: 12137824]
25. Schiepers C, Hoh CK, Nuyts J, et al. 1-11C-acetate kinetics of prostate cancer. J Nucl Med. 2008; 49(2):206–215. [PubMed: 18199613]

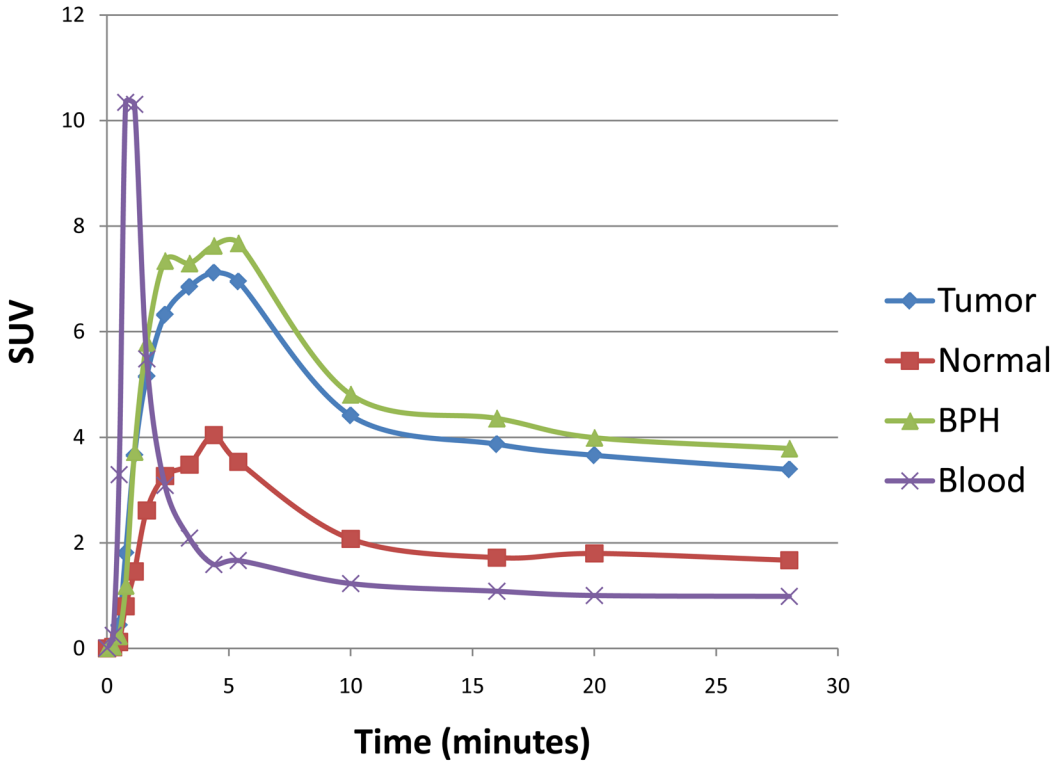

Figure 1.
Time activity-curve representing the mean of all patients, using iliac artery (red), prostate tumor (blue), benign prostatic hyperplasia (BPH) foci (purple) and normal prostate (green). Uptake is expressed in SUV (standardized uptake value). Tumor and BPH foci showed rapid uptake of ^{11}C-Acetate in the prostate peaking ~3–5 minutes, followed by a relatively plateau after 10 minutes.

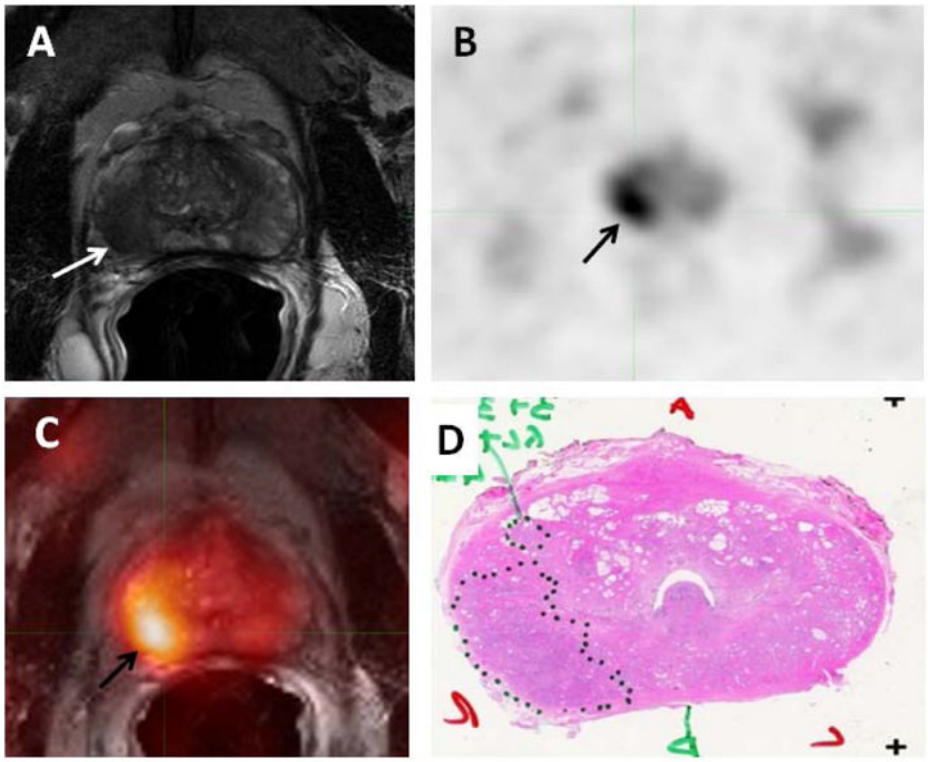

Figure 2.

58-year-old male with prostate cancer. Axial T2-weighted MRI **(A)** demonstrates a low signal intensity focus in the right mid gland peripheral zone (white arrow), which shows ^{11}C-Acetate uptake in the axial PET image (black arrow) **(B).** Fused ^{11}C-Acetate PET/MRI **(C)** better localizes the tumor (black arrow). Corresponding pathology shows a Gleason 3+4 tumor in the right mid-peripheral zone (inked in black) **(D).**

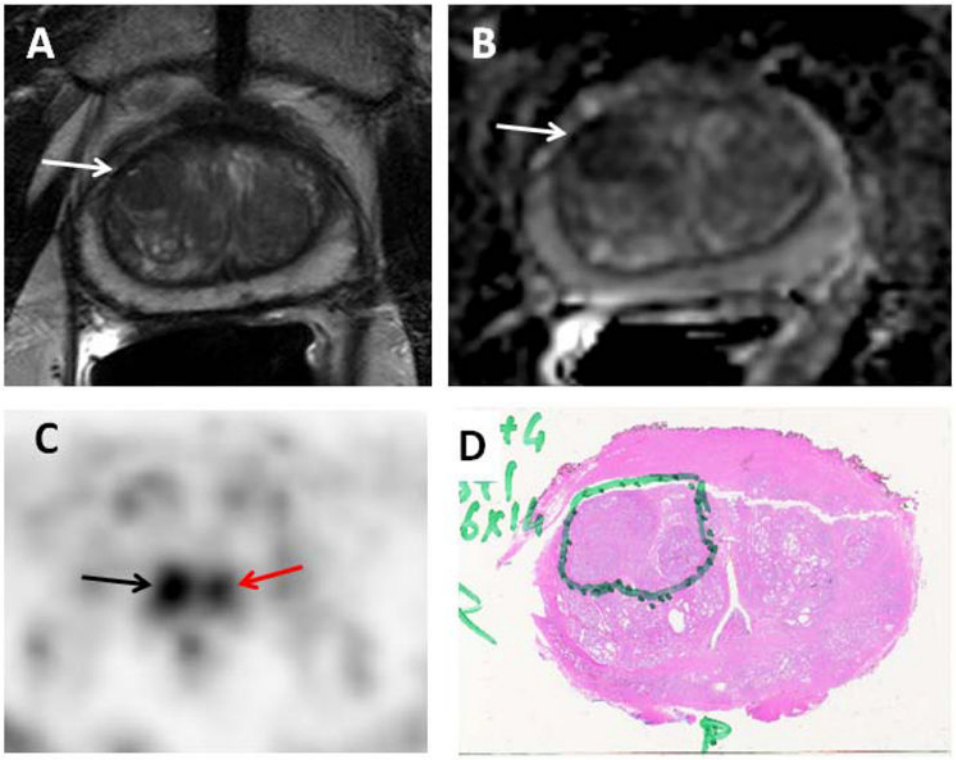

Figure 3.
69 year-old-male with prostate cancer. Axial T2-weighted MRI **(A)** and ADC map **(B)** show focal low signal intensity in the right mid-anterior central gland (white arrows), which demonstrates increased ^{11}C-acetate uptake (black arrow) **(C).** Corresponding pathology **(D)** confirms the presence of tumor (Gleason 4+4), inked in green. Focal ^{11}C-acetate uptake in the left central gland corresponds to a BPH nodule (red arrow) **(C).**

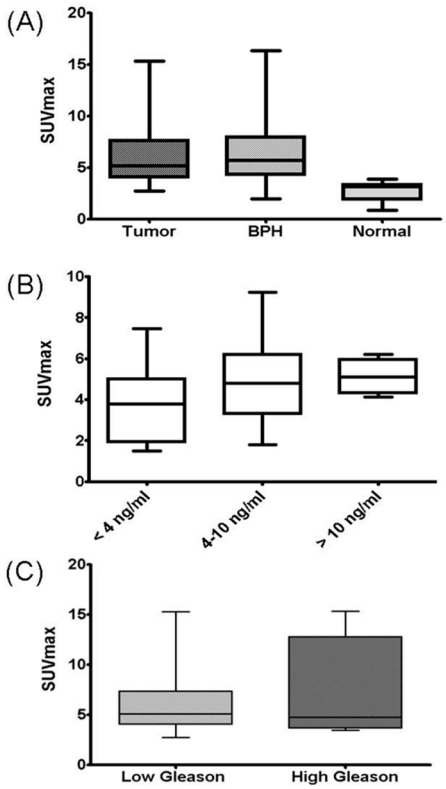

Figure 4.

(A) Prostate tumors and benign prostatic hyperplasia (BPH) showed similar ^{11}C-acetate uptake (p=0.757), while the SUV in normal prostate areas was significantly lower than tumor (p<0.0001). **(B)** No significant correlation was noted between SUV and serum PSA levels (r = 0.257) or **(C)** between ^{11}C-Acetate uptake of lesions with lower Gleason scores (3+4 and below) and lesions with higher Gleason scores (4+3 and above), (p=0.064).

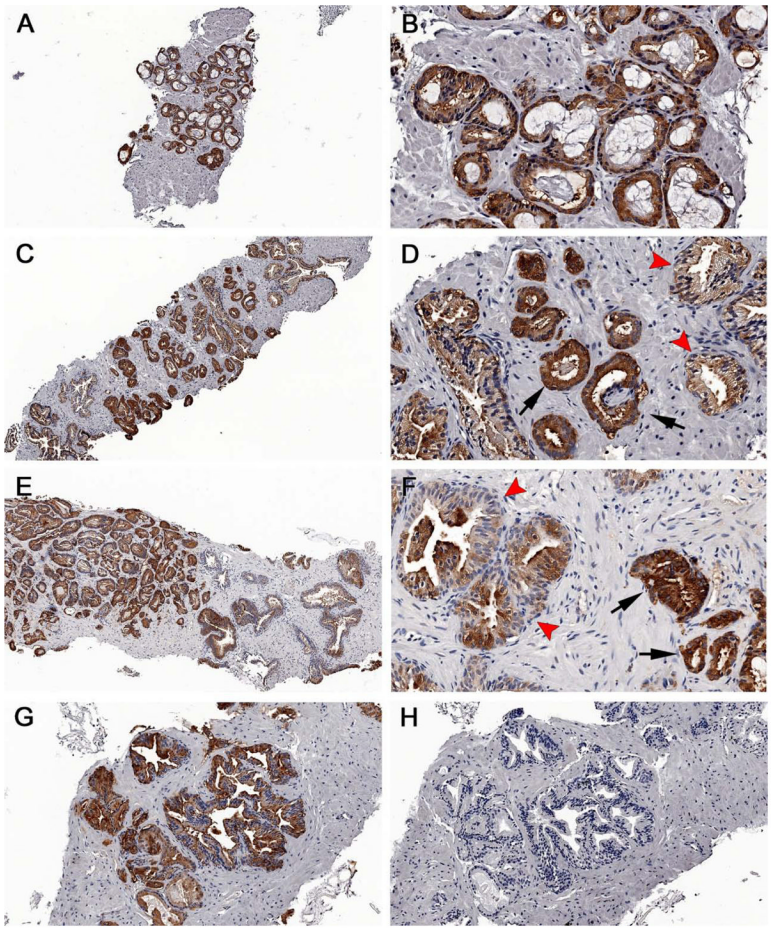

Figure 5.

Immunohistochemical staining of fatty acid synthase in prostate cancers. Both ^{11}C-acetate negative and positive cases were stained. Note the intense brown staining of most cells against the background stroma in most of the specimens, which can be recognized even at low power **(A, C, E).** Discrete differences in staining intensity were seen between benign tissue **(arrowheads)** and tumor **(arrows);** however no difference was seen between (**A–D)** ^{11}C-acetate-negative cases and **(E–G)** ^{11}C-acetate-positive cases. Negative controls showing no FAS staining **(H).** Magnification: **(A, C, E)=**5X; **(B, D, F)**=20X; **G–H**=10X.

Table 1

Logan graphical analysis parameters in tumor, BPH and normal prostate.

	Vd (r-value)	DVR (r-value)
Tumor	3.0 (0.999)	2.0 (0.999)
BPH	3.4 (0.997)	2.3 (0.999)
Normal prostate	1.4 (0.997)	---------